ACS APPLIED MATERIALS & INTERFACES

Research Article

www.acsami.org

Micromechanics of TEMPO-Oxidized Fibrillated Cellulose Composites

Mindaugas Bulota,*[,†] Supachok Tanpichai,[‡] Mark Hughes,[†] and Stephen J. Eichhorn*[,‡,§]

[†]Department of Forest Products Technology, School of Chemical Technology, Aalto University, P.O. Box 16400, 00076-Aalto, Finland

[‡]Materials Science Centre, School of Materials and the Northwest Composites Centre, School of Materials, University of Manchester, Manchester M13 9PL, United Kingdom

[§]College of Engineering, Mathematics and Physical Sciences, University of Exeter, Harrison Building, North Park Road, Exeter, EX4 4QF, United Kingdom

ABSTRACT: Composites of poly(lactic) acid (PLA) reinforced with TEMPO-oxidized fibrillated cellulose (TOFC) were prepared to 15, 20, 25, and 30% fiber weight fractions. To aid dispersion and to improve stress transfer, we acetylated the TOFC prior to the fabrication of TOFC-PLA composite films. Raman spectroscopy was employed to study the deformation micromechanics in these systems. Microtensile specimens were prepared from the films and deformed in tension with Raman spectra being collected simultaneously during deformation. A shift in a Raman peak initially located at ~1095 cm^{-1}, assigned to C−O−C stretching of the cellulose backbone, was observed upon deformation, indicating stress transfer from the matrix to the TOFC reinforcement. The highest band shift rate, with respect to strain, was observed in composites having a 30% weight fraction of TOFC. These composites also displayed a significantly higher strain to failure compared to pure acetylated TOFC film, and to the composites having lower weight fractions of TOFC. The stress-transfer processes that occur in microfibrillated cellulose composites are discussed with reference to the micromechanical data presented. It is shown that these TOFC-based composite materials are progressively dominated by the mechanics of the networks, and a shear-lag type stress transfer between fibers.

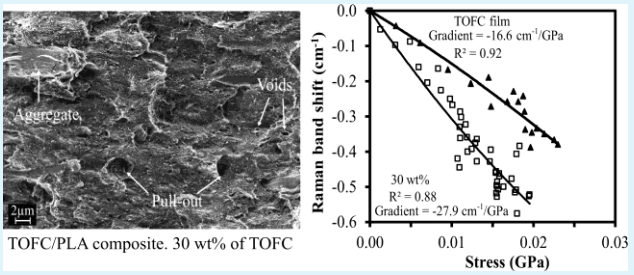

TOFC/PLA composite. 30 wt% of TOFC

KEYWORDS: *TEMPO-mediated oxidation, fracture mechanics, nanocomposites, Raman Spectroscopy, cellulose*

INTRODUCTION

Biobased materials have attracted attention in recent years because of increasing environmental concerns. The majority of commodities are, however, still produced from nonrenewable resources, which create challenges in waste management and contribute to landfill. There is therefore a strong demand for compostable materials based on renewable resources. Cellulose is abundant, renewable and biodegradable and as such cellulose fiber reinforced nanocomposites are currently receiving much attention. Nature has evolved plant-based nanocomposites by manipulating three main polymers: cellulose, hemicelluloses, and lignin. The function of cellulose in these natural nanocomposites is that of reinforcement, with hemicelluloses and lignin acting as the matrix.[1] The high strength and stiffness of cellulose can potentially be utilized to create synthetic cellulose reinforced composites. To engineer such nanocomposite materials with desirable mechanical properties, it is essential to understand the underlying micromechanical mechanisms controlling their behavior. The physical handling of nano and microfibrils is, however, challenging. Thus conventional tools for studying micromechanics cannot be directly applied to cellulose reinforced nanocomposites. Raman spectroscopy has been shown to be a useful, noninvasive, tool for studying the in situ micromechanics of polymers,[2,3] particulate composites,[4,5] carbon nanotube reinforced composites,[4,6] and cellulosic materials such as wood fibers,[7,8] hemp fibers,[9,10] cotton,[11] and cellulosic nanocomposites.[12−15]

The use of Raman spectroscopy to study deformation in polymer single crystals was pioneered by Mitra and coworkers.[16] They concluded that frequency shifts in the spectra obtained from single crystals of diacetylene take place due to bond anharmonicity. A later study by Batchelder and Bloor[17] supported the findings of Mitra and colleagues. As cellulose crystallites are stretched along the axis, the skeletal chain is deformed, mainly by ring deformation in conjunction with stretching and bending of the β-1,4-glycosidic linkage, as well as stress distribution via hydrogen bonding.[18,19] As a result, a Raman band initially located at ~1095 cm^{-1}, assigned to C−O−C stretching,[7,20] shifts toward a lower wavenumber position, due to direct deformation of the cellulose backbone[8,9,21−23]

Natural fibers such as flax and hemp possess many physical flaws that are known to have a negative effect on their mechanical properties.[22,24] Moreover, when these fibers are used as composite reinforcements, they[22,24] act as stress

Received: October 11, 2011
Accepted: December 19, 2011
Published: December 19, 2011

concentrators, and initiation sites of fiber-matrix debonding.[25] According to classical theory on the mechanics of materials,[26] the influence of the flaws should be reduced by breaking down the fibers into nano fibrils, because statistically fewer flaws ought to occur in thinner fibers. Significant energy and mechanical action is however required to evolve nanosized cellulose fibers, which may actually be detrimental to the mechanical properties of the material. Cellulose oxidation by a 2,2,6,6-tetramethylpiperidine-1-oxyl radical (TEMPO) is a relatively new method facilitating mechanical disintegration of cellulose fibers into nano fibrils, reducing energy and mechanical action. This process, pioneered by Isogai and co-workers, has been well-reviewed.[27]

The modulus of TEMPO-oxidized cellulose prepared from tunicate has been reported to be 145 GPa.[28] This value agrees well with a value of 143 GPa reported by Sturcova et al.[29] and approaches the theoretical Young's modulus of cellulose which, depending upon the model used, ranges from approximately 124 to 172 GPa.[18,30,31] Recently, using quantum mechanics, the modulus of cellulose I beta has calculated to be 99.7 GPa.[32] Understanding the micromechanics of TEMPO-oxidized cellulose reinforced composites could help tailor the properties of cellulose, as well as that of the composite.

The aim of the present study was to investigate how stress transfer in TEMPO-oxidized cellulose reinforced poly(lactic) acid (PLA) composites is influenced by the amount of reinforcement present in the composite. The cellulose was acetylated prior to the preparation of the composites in order to enhance fiber dispersion and improve fiber-matrix adhesion. Raman spectroscopy was employed to study in situ molecular deformation, and to gain insight into the stress transfer process. The effect of the weight percent load of reinforcement on the stress transfer in the composites was studied. This study contributes to a broader set of studies investigating deformation mechanisms in nano cellulose reinforced composites and contributes to a better understanding of these materials.

MATERIALS

TEMPO-oxidized cellulose fibrils were prepared from bleached birch Kraft pulp according to the method detailed by Saito and co-workers.[33] After the oxidation, the fibrils were stirred in a commercial blender with the addition of deionized water until a transparent gel was formed. No additional filtration, or any other treatment, was carried out. This mixture of fibrillated cellulose is hereafter referred to as TEMPO-oxidized fibrillated cellulose (TOFC). Commercially available PLA, poly(lactic) acid, (NatureWorks 2002D) was used as the matrix. PLA is a biobased polymer synthesized from lactic acid.[34]

METHODS

3.1. Acetylation. The acetylation reaction involves esterification of hydroxyl groups and is commonly used to increase the hydrophobicity of natural plant fibers[35] and wood.[36] TOFC as well as bleached birch Kraft pulp used (as a reference) was acetylated with acetic anhydride in order to increase hydrophobicity, and thus improve dispersion in nonpolar solvents such as chloroform.

A solvent exchange procedure was carried out first of all to facilitate the acetylation of TOFC and second to obtain a suspension of TOFC in chloroform, since PLA is soluble in chloroform. 120 g of a suspension of TOFC in water, having a solids content of 0.5% by weight was solvent exchanged, in three sequential centrifugations at 8000 rpm for 15 min at 20 °C, to dimethylformamide (DMF). The suspensions were sonicated for 2 min prior to the acetylation reaction, which was carried out by adding 50 g of acetic anhydride (AA) to the TOFC suspension in DMF. The TOFC in DMF was preheated to 125 ± 5 °C prior to the addition of AA, and kept at this temperature for 30 min in order to boil away any remaining water. Then the suspension was cooled down to approximately 50 °C and AA added. Approximately 1 g of dry cellulose was treated with 80 g of AA. The reaction took place in a round-bottom flask at 125 ± 5 °C for 45 min. Then the reaction was quenched by placing the reaction flask into an ice bath. Subsequently, 50 g of acetone was added, the mixture centrifuged, and the remaining reagent, byproduct (acetic acid) and solvents decanted-off. Additional acetone (50 g) was added and the suspension left overnight, after which it was solvent exchanged to acetone, and from acetone to chloroform by 2 centrifugations as already described. Before each centrifugation the suspensions were sonicated for 2 min.

3.2. Determination of DS. The degree of substitution of acetyl groups was determined by conducting a standard saponification reaction followed by titration (known as the Eberstadt method). This method has been well reviewed by Murray et al.[37] and is described in detail by Tanghe et al.[38] It is based on the cleavage of ester groups by saponification followed by titration with hydrochloric acid (HCl). The volume of sodium hydroxide (NaOH) consumed during saponification indicates the degree of substitution. Acetyl content was calculated using eq 1[39]

$$\text{acetyl content (\%)} = ((D - C)N_a + (A - B)N_b)(4.035/W) \quad (1)$$

where A is the volume of NaOH (mL) added to the sample, B is the volume of NaOH (mL) added to the blank, C is the volume of HCl (mL) added to the sample, D is the volume of HCl (mL) added to the blank, W is the weight of sample (g), and N_a and N_b are the normality of HCl and NaOH solutions, respectively. The average number of acetyl groups per anhydro-D-glucose unit of cellulose, i.e., degree of substitution (DS) can be calculated from eq 2:[40]

$$DS = (3.86 \cdot \text{acetyl content (\%)})/(102.4 - \text{acetyl content (\%)}) \quad (2)$$

The presence of carboxylic acids (COOH) as a result of TEMPO oxidation affects the final value of the acetyl content determined by the Eberstadt method. It is overestimated if nonmodified pulp is used as reference material since NaOH reacts with COOH in forming sodium carboxylate salt (COONa). Therefore TEMPO-oxidized cellulose was used as a blank sample in eq 1 for calculating the DS of acetylated TOFC.

3.2. Fourier Transform Infrared Spectroscopy (FT-IR). The FT-IR spectra of dried TOFC, acetylated TOFC as well as bleached birch Kraft pulp, and acetylated bleached birch Kraft pulp were collected using a FTS 600 (Bio-Rad Laboratories, Inc., Hercules, CA, USA) spectrometer, equipped with a laser operating at a wavelength of 632.8 nm. The samples were placed in a photoacoustic cell and the spectra recorded between 400 and 4000 cm^{-1}. Three points having the lowest intensity were selected from the spectrum and the baseline was created by linear interpolation between these points. Then the baseline was subtracted from the spectrum.

3.3. Atomic Force Microscopy (AFM). TOFC suspensions of approximately 0.1 wt % in DMF and in water as well as acetylated TOFC suspensions in acetone and in chloroform were centrifuged (8000 rpm for 45 min at 20 °C) and the supernatant (0.01 wt %) spin coated on a silica substrate (3000 rpm for 1 min at room temperature). Acetylated TOFC was spin coated on a mica substrate. The substrate was treated with polyethylene imine (PEI) which is positively charged thus facilitating adsorption of negatively charged cellulose on the substrate. The films were imaged in tapping mode with a Nanoscope IIIa multimode scanning probe AFM (Digital Instruments Inc., Santa Barbara, CA, USA). Silicon cantilevers (NSC15/AIBS, MicroMasch, Tallin, Estonia) were used to perform the imaging at a frequency of 300−360 kHz. The radius of the tips, according to the manufacturer, was ~10 nm.

3.4. Preparation of Composite Films. A 0.3% suspension by weight of acetylated TOFC in chloroform was mixed with PLA

dissolved in chloroform. The concentration of the PLA solution was 2% by weight. The required amount of acetylated TOFC was added to achieve composites with 15, 20, 25 and 30% weight fractions, based on dry weight of TOFC. The mixture of TOFC and PLA was homogenized with a Polytron PT2100 homogenizer (Kinematica, Inc., Lucerne, Switzerland) for 5 min and degassed before casting onto a release agent (Chemlease 75, Chem-Trend L.P., Howell, MI, USA) treated glass plate. Unreinforced PLA films were also cast from solution. The casts were left in a well-ventilated room overnight. Pure TOFC films were prepared by casting an acetylated TOFC suspension (0.3 wt %) in chloroform onto a glass Petri-dish. After evaporation of chloroform, several drops of deionized water were dispersed onto the film in order to peel it off from the glass surface. All films were finally dried in an oven at 60 °C for 30 min. Thickness of the films varied between 80 and 90 μm for the pure PLA and composite films. The pure cellulose film had a thickness of ~50 μm.

3.5. Raman Spectroscopy and Micromechanics. Rectangular composite specimens (30 × 2 mm^2) were cut out from the films using a razor blade. An optical microscope was used to measure the width of the samples and digital calipers to evaluate the thickness. The tensile specimens were deformed in tension in a miniature tensile testing instrument (Deben Microtest, Deben, Bury St Edmonds, U.K.). The gauge length was 20 mm and the loading speed 0.05 mm min^{-1}. Raman spectra were collected using a Renishaw 1000 spectrometer equipped with a 785 nm wavelength laser. This spectrometer was coupled to an Olympus (BH-1) microscope fitted with a × 50 magnifying objective lens. The laser beam was polarized parallel to the axis of the sample. When focused on the surface, the spot size was ~2 μm. Each spectrum was recorded using an exposure time of 10 s with four accumulations, i.e., a total of 40 s. The samples were loaded stepwise and the strain increment in between each measurement was 0.1%. The peak position of a Raman band initially located at ~1095 cm^{-1} was determined using a mixed Gaussian/Lorentzian function, and an algorithm based on the work of Marquardt.[41] At least five samples were tested for each type of composite, and the pure acetylated TOFC films.

The orientation of fibrils within a composite film was measured by rotating the samples by 5° angular increments from 0 up to 360°. The intensity of the Raman peak located at ~1095 cm^{-1} was recorded at each rotation increment.

3.6. Scanning Electron Microscopy (SEM). Fractured tensile specimens were gold sputtered in a BAL-TEC SCD 050 (Capovani Brothers Inc., Scotia, NY, USA) sputter coater at 40 mA current for 15 s. Then, the cross sections were imaged with a Zeiss Supra 40 (Carl Zeiss AG, Germany) scanning electron microscope, equipped with a Schottky electron gun and an in-lens secondary electrons detector.

RESULTS AND DISCUSSION

4.1. Acetyl Content. The acetyl content of acetylated TOFC calculated using eq 1 was 3.9% which, by applying eq 2, translates to a DS of 0.16. By following the same procedure, the acetyl content of acetylated birch Kraft pulp was determined to be 2.9% and the DS 0.11.

4.2. Fourier Transform Infrared Spectroscopy (FT-IR). Figure 1 shows the FT-IR spectra of TOFC and acetylated TOFC as well as acetylated birch bleached pulp and nonacetylated birch bleached pulp.

The band appearing at 1608 cm^{-1} following TEMPO oxidation corresponds to sodium carboxylate (COONa),[42] indicating successful oxidation of hydroxyl groups. The appearance of the 1735 cm^{-1} band upon acetylation of both the pulp and TOFC indicates the presence of carbonyl (C═O) groups,[43] indicative of esterification. Additionally a peak at 1365 cm^{-1}, corresponding to methyl C−H symmetric bending,[44,45] is seen for the birch pulp, which could be due to the presence of hemicelluloses. Because most of the hemicelluloses are removed during TEMPO oxidation the peak significantly

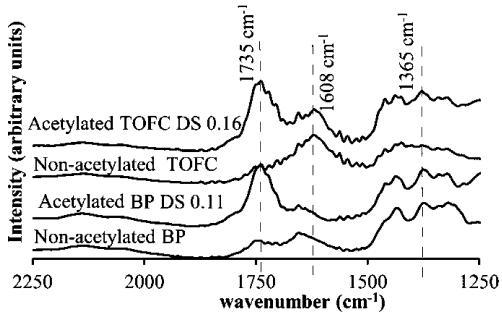

Figure 1. FT-IR spectra of birch pulp (BP), acetylated birch pulp, TOFC, and acetylated TOFC.

diminishes in intensity (Figure 1). The presence of this peak in acetylated TOFC indicates the presence of acetyl groups providing strong evidence that the TOFC has been successfully esterified.

4.3. Morphology of TOFC Using Atomic Force Microscopy (AFM). Atomic force microscopy (AFM) was employed to study the morphology of TOFC spin coated from the supernatant after centrifugation and its behavior in different

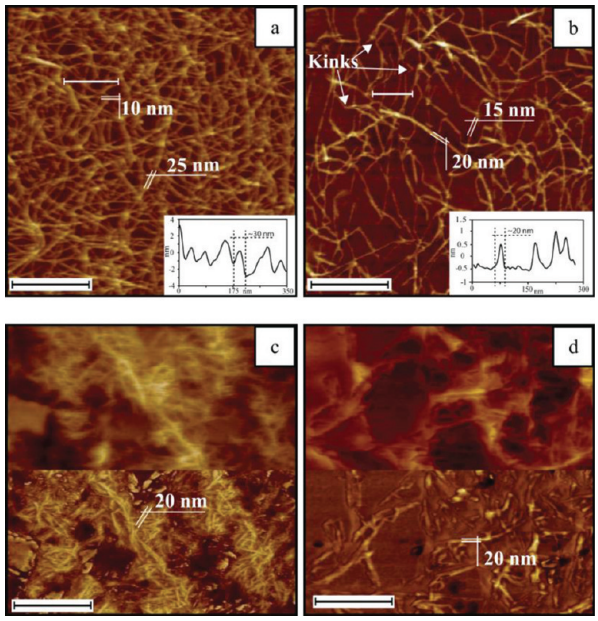

Figure 2. AFM topography images of spin coated: (a) TOFC in water, (b) TOFC in DMF, (c) acetylated TOFC in acetone, and (d) acetylated TOFC in chloroform (topography combined with phase image, upper and lower images, respectively). Scale bar is 500 nm. The presence of kinks in the fibrils is clearly seen in b. The insets in a and b show the height profiles of the marked (white line) areas.

media. Figure 2 shows TOFC at different stages of composite preparation.

An AFM image of TOFC in water, before starting the solvent exchange procedure, is shown in Figure 2a. The width of the fibrils was approximately 10−15 nm and their length in the region of 1 μm, giving an aspect ratio of around 100. Similar dimensions were confirmed by the height profile images, shown in the insets in Figure 2a,b. The fibrils observed in Figure 2b exhibited some kinks (identified on the image). Such features have been previously reported[33] and considered to reduce the

dx.doi.org/10.1021/am201399q | ACS Appl. Mater. Interfaces 2012, 4, 331−337

effective aspect ratio of the fibrils. What is notable in Figure 2b is the good dispersion of TOFC in DMF due to the presence of sodium carboxylate groups. A change of the media led to aggregation of the nano fibrils (Figure 2c,d), but nevertheless, individual nanosized fibrils can still be distinguished in the AFM images. Height profiles are not presented in Figure 2c,d because they would not provide any further information regarding the width of fibrils, because of aggregation. The aspect ratio, however, is significantly lower, and the TOFC resembles nanorods.

4.4. Raman Spectroscopy and Micromechanics. Typical Raman spectra of the pure PLA, acetylated TOFC films and composites with 15 and 25 wt % of acetylated TOFC are presented in Figure 3.

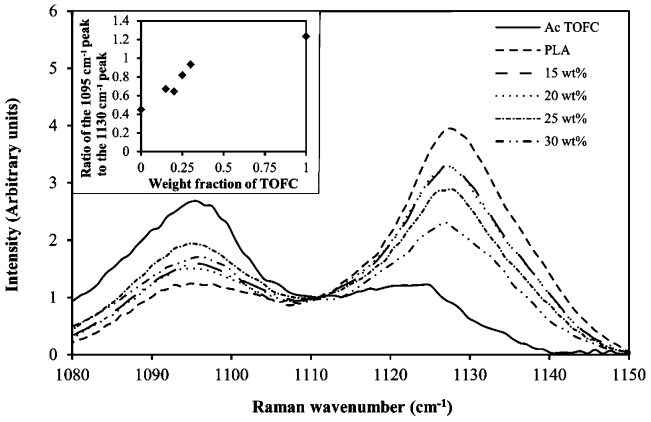

Figure 3. Typical Raman spectra of pure acetylated TOFC film, pure PLA film and composites with 15, 20, 25, and 30 wt % TOFC at 0% strain. Inset shows the ratio of the intensity of the Raman peak located at ~1095 cm^{-1} to that of the peak located at ~1130 cm^{-1} as a function of the weight fraction of TOFC.

The Raman band located at ~1130 cm^{-1} is characteristic of PLA, and a band located at ~1095 cm^{-1} is characteristic of cellulose. Although there is a small intensity located at ~1095 cm^{-1} due to PLA, it is thought to not affect the positioning of the cellulose band as its intensity significantly increases upon the addition of cellulose[46] (Figure 3). The relative band intensities corresponding to TOFC and PLA change with respect to the weight fraction of cellulose added, indicating a systematic change in this parameter. The ratio of the intensity of the Raman band located at ~1095 cm^{-1} to the intensity of the band located at ~1130 cm^{-1} is plotted against the weight fractions of TOFC in the composites, and is shown in the inset of Figure 3. The difference in intensity ratio between composites containing 15 and 20 wt % of TOFC was negligible, though the change is more pronounced as the weight fraction of TOFC increases. This gives a way of evaluating the actual weight fraction of the reinforcement, and provides a potential method for determining variability in weight fraction, within a sample to a spatial resolution of 1−2 μm (the approximate size of the laser spot).

The variation of the intensity of the Raman band located at ~1095 cm^{-1} as a function of rotation angle, is shown in Figure 4 for a composite sample containing 25 wt % of cellulose. The incident laser light is polarized parallel to the main axis of the samples (dashed line in Figure 4). If the fibril orientation (and thus the orientation of the cellulose molecular chains) is parallel to this direction then the intensity recorded from the sample is

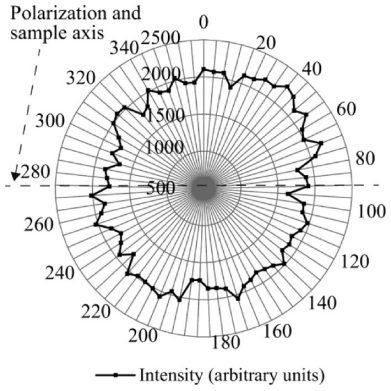

Figure 4. Intensity (radial axis) of the Raman band located at ~1095 cm^{-1} as a function of the rotation angle (angular axis) of a TOFC/PLA composite with respect to the polarization direction of the spectrometer laser and the sample's main axis (25 wt % composite shown).

highest. Since the intensity of the Raman band located at ~1095 cm^{-1} with respect to the sample orientation is representative of the distribution of the fibrils within the sample, the low variation in intensity with rotation angle seen in Figure 4 indicates a random and uniform distribution of TOFC fibrils within the PLA matrix.

Composites with different weight fractions of reinforcement were deformed and Raman spectra recorded. Figure 5 shows

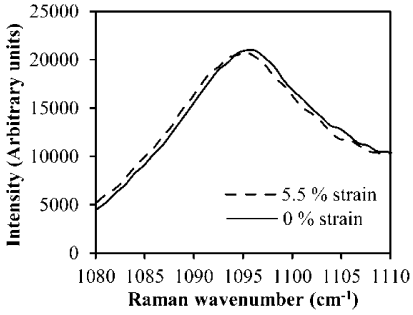

Figure 5. Typical deformation induced shift at of the Raman band from cellulose located at ~1095 cm^{-1} for an acetylated TOFC composite (30 wt %).

typical Raman spectra for an acetylated TOFC reinforced composite (30 wt %) before and after deformation (5.5% strain). The Raman band located at ~1095 cm^{-1} is observed to shift towards a lower wavenumber; by 0.6 cm^{-1} with a strain of 5.5%.

The shift (Figure 5) itself (presented as a gradient) indicates molecular deformation of the cellulose backbone upon the deformation of the composite due to stress transfer from the matrix to the reinforcing phase. Typical shifts in the Raman band located at ~1095 cm^{-1} with respect to strain and weight fractions of TOFC, in all composite samples are presented in Figure 6. Data obtained from composite samples are compared against those obtained from pure acetylated TOFC films, without the presence of PLA resin. Scatter in the data is more pronounced for composite films with lower amounts of cellulose, because of weaker signals obtained from these materials.

The magnitude of the shift (presented as a gradient) of the Raman band located at ~1095 cm^{-1} with respect to strain for

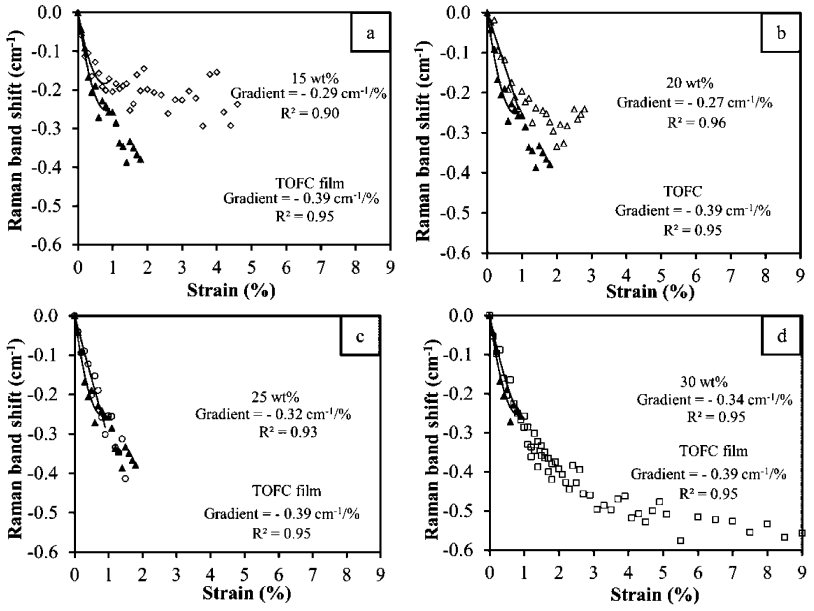

Figure 6. Shifts in the peak position of the Raman band located at ~1095 cm^{-1} for TOFC/PLA composites with different weight fractions of acetylated TOFC: (a) 15, (b) 20, (c) 25, and (d) 30% as a function of strain (unfilled symbols) compared with data obtained from pure acetylated TOFC films (filled triangles). Data are fitted (up to a strain of 0.9%) using a quadratic equation (solid lines) and the slopes determined from the first derivative of this fit solved at a strain = 0.3%.

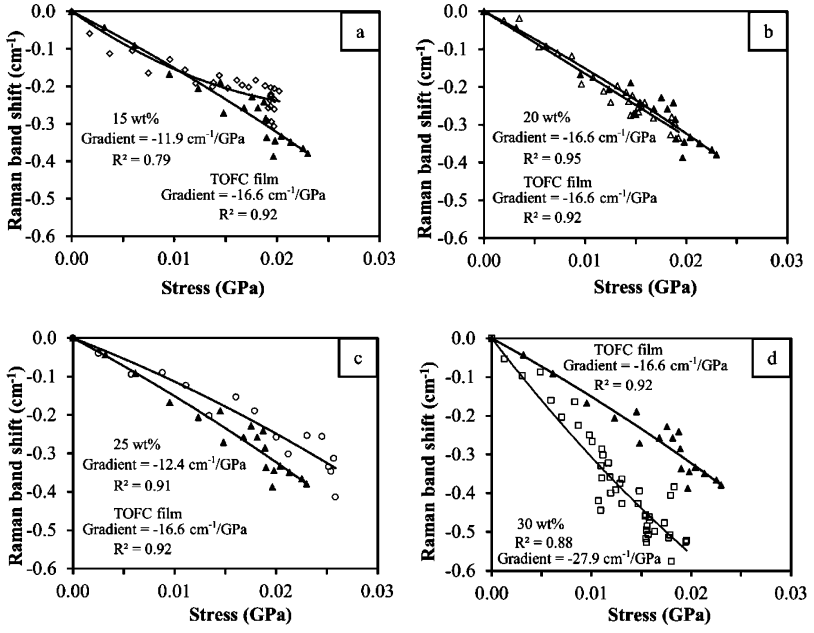

Figure 7. Typical shifts in the Raman band located at ~1095 cm^{-1} for composites with different weight fractions of acetylated TOFC: (a) 15, (b) 20, (c) 25, (d) 30% as a function of stress (unfilled symbols) compared to shifts in pure acetylated TOFC film (filled triangles). Data are fitted using a quadratic equation and the slopes determined from the first derivative of this fit solved at a stress = 0.01 GPa.

the composite materials increases as the weight fractions of reinforcement agent increases (from 0.29 to 0.34 cm^{-1} $\%^{-1}$ with an increase in weight fraction of 15 to 30%). The shift rate with respect to strain, for a uniform stress structure, would be proportional to the modulus of the material.[47] For a uniform strain type structure (i.e., a composite) the shift rate with respect to strain ought to be independent of modulus.[47] We note that at lower weight fractions the initial shift rates with respect to strain are significantly lower than for pure sheets of TOFC. The shift rates effectively converge at higher volume fractions, suggesting that the stress-transfer becomes dominated by the network mechanics (i.e., fiber−fiber interactions and a uniform strain deformation). Highly packed and high density networks, such as the ones envisaged to be generated here and existing in the composites at higher volume fractions, are expected to show Cox-like uniform strain behavior.[48] This will lead to stress transfer processes akin to a "composite within a composite". Weight-dependent maxima strengths for dense fibrous networks (paper) have been observed, and attributed to Cox-like stress transfer[49] within the networks themselves. We show a progressive convergence (from Figure 6a−d) of the micromechanical behavior of the pure networks of TOFC, and

the composite materials, as the network mechanics become more dominant. The lower shift rate with respect to strain observed in composites with 15 and 20 wt % of acetylated TOFC compared to pure TOFC sheets could be indicative of poor stress transfer to the fibrils. It could however be that a volume fraction threshold has not been met for the fibrous networks in these materials, and that therefore the stress-transfer mechanisms are different, as already stated.

It is also noted that the strain to failures for composites with 15 and 30 wt % of TOFC are approximately twice that of the pure cellulose film (Figure 6a, d), indicating frictional sliding during deformation. This proposed frictional sliding mechanism exhibits itself as a plateau in the shift rate at higher strains (>1%) compared to pure acetylated TOFC film. The strain to failure is more than five times higher for the composite with 30 wt % of TOFC compared to the pure acetylated TOFC film although not all of the 30 wt % load samples were strained to the point of failure. The high strain to failure exhibited by the 30 wt % TOFC composites may be due to pull-out of fibrils within the bulk of the network, which are not well-bonded to the surrounding resin. Similar micromechanical behavior has been observed in porous nanofibril structures, where voids facilitated interfibrilar debonding and slippage.[50] It has been shown experimentally that the Raman band located at ~1095 cm^{-1} shifts at a rate, with respect to strain, of −2.4 cm^{-1}/% for tunicate cellulose/epoxy composite samples.[29] The shift values observed in our study were much lower - approximately 0.34 cm^{-1}/% in a 30 wt % composite and 0.29 cm^{-1}/% in a 15 wt % composite. This could indicate an inefficient stress transfer from matrix to cellulose fibrils, due to an effective decrease in the aspect ratio due to aggregation, or to lower crystallinity of the cellulose fibrils. Even though the dispersion of cellulose was good, further aggregation of fibrils within the matrix could have prevented the reinforcement from being more effective. Additionally, the interaction between the matrix and fibrils may not have been sufficient to effectively transfer the stress from the matrix to the reinforcement.

The dependency of the shift rates with respect to stress are slightly different to values seen with respect to strain. Very little difference is noted between composites produced with 15, 20, and 25% TOFC and a pure film of acetylated TOFC. Initially, the data appear to superimpose, with deviations only occurring at higher levels of stress (Figure 7). Complete agreement between data sets for composites is observed for the sample reinforced with 20 wt % and the pure TOFC film. Deviations between the slopes in the data may be due to the pull-out mechanisms previously reported, or to other mechanisms leading to inefficient stress transfer between the matrix and the fibers.

The band shift rate of the Raman band located at ~1095 cm^{-1} with respect to stress for the composite containing 30 wt % TOFC is however ~80% higher than for the pure acetylated TOFC film, and is the highest of all the composites studied (Figure 7d). This implies that stress is transferred both through fibril−fibril interactions and from the matrix to the fibrils in an efficient manner. It is probable then that the percolation threshold in these types of composite is very high, since effective stress transfer is achieved only at 30 wt % of TOFC. The mechanism for this enhanced stress transfer could be that the consolidated network within the composite is acting in a Cox-like manner, as previously suggested, and the network mechanics therefore dominate the stress-transfer process.

4.3. Fracture surfaces. Images of the fractured surfaces of the composites are shown in Figure 8. Figure 8a shows the

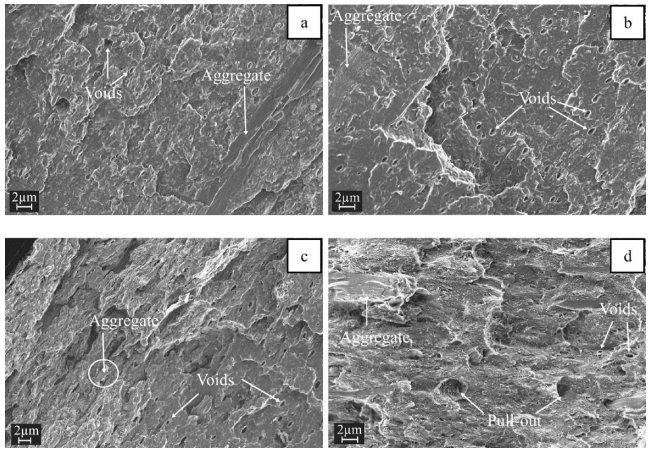

Figure 8. Typical SEM micrographs of composite fracture surfaces with: (a) 15, (b) 20, (c) 25, (d) 30 wt % load of TOFC.

fracture surface of a 15 wt % composite. The surface is indicative of a clean brittle fracture, since there is little evidence of plastic deformation (e.g., yield) of the matrix. The aggregate fibril structure observed on the right-hand side of Figure 8a does not appear to have debonded from the matrix, implying a good fibril-matrix interaction. The composites with 20 and 25 wt % of acetylated TOFC, appear to exhibit more permanent material deformation and stepping of the fracture surface, compared to the 15 wt % composite (Figure 8b,c). Also visible in these images are the voids and TOFC aggregates. However, there is no indication of large clustered aggregates which would effectively reduce reinforcement due to their lower aspect ratio. Figure 8d shows the fracture surface of a 30 wt % composite. There is more evidence of pull-out indicating a stress build-up exceeding the fiber-matrix bond strength. This pull-out mechanism could be the cause of the enhanced strain to failure seen for the 30 wt % composite (cf. Figure 8d).

Some voids are present in the 30 wt % composite, which could have been produced by the pull-out a TOFC aggregate. Although, aggregates which are still visible did not debond from the matrix and fracture occurred within them. This supports the initial notion of a good fiber − matrix interaction and suggests that acting stresses in the 30 wt % composite are higher in comparison to the composites, containing lower weight fractions of TOFC. Thus the shift rate of the Raman band is higher at larger weight fractions of TOFC (Figures 6 and 7).

CONCLUSIONS

Raman spectroscopy has shown to be an appropriate tool for investigating the micromechanics of acetylated TOFC reinforced composites. Despite modification AFM showed extensive aggregation of acetylated TOFC and an accompanying decrease in the aspect ratio of the reinforcement when suspended in both acetone and chloroform. This is most probably the result of incomplete acetylation. Nevertheless, the dispersion of fibrils was found to be random and uniform, as shown by the invariant intensity of the Raman band located at ~1095 cm^{-1} as a function of rotation angle of the specimens. The micromechanics of the composites were investigated using Raman spectroscopy. Composites with 15 wt % load of TOFC appeared to exhibit poor stress transfer with debonding taking

place at the fiber-matrix interface at strains below 1%. The stress transfer mechanism appears to alter as the weight fraction of TOFC increases, most probably due to the formation of nascent network, which at 30 wt % load of TOFC acts in a Cox-like manner due to the formation of a fully consolidated network. Thus the most efficient stress transfer was observed at 30 wt % resulting from the dominating network mechanisms. The study indicates that the percolation threshold of these materials is high.

AUTHOR INFORMATION

Corresponding Author

*E-mail: mindaugas.bulota@aalto.fi (M.B.); s.j.eichhorn@exeter.ac.uk (S.J.E.) Tel.: +358 5 056 70506 (M.B.); +44 1392 725515 (S.J.E.).

ACKNOWLEDGMENTS

The authors thank the Academy of Finland (decision number 127609) and Finnish Cultural Foundation (Grant 00100101) for the financial support of Mindaugas Bulota and the Royal Thai Government for support of Supachok Tanpichai. The travelling costs were partially covered by COST action FP0802. We are also grateful to Rita Hatakka for recording the FT-IR spectra and Anna Olszewska for AFM images. Many thanks are due to Tuomas Hänninen for providing TEMPO-oxidized cellulose and valuable discussions.

REFERENCES

(1) O'Sullivan, A. *Cellulose* **1997**, *4*, 173−207.
(2) Young, R. J.; Day, R. J.; Zakikhani, M. *J. Mater. Sci.* **1990**, *25*, 127−136.
(3) Davies, R. J.; Montes-Moran, M. A.; Riekel, C.; Young, R. J. *J. Mater. Sci.* **2001**, *36*, 3079−3087.
(4) Cooper, C A.; Young, R. J. *J. Raman Spectrosc.* **1999**, *30*, 929−938.
(5) Shyng, Y.; Bennett, J.; Young, R. J.; Davies, R.; Eichhorn, S. J. *J. Mater. Sci.* **2006**, *41*, 6813−6821.
(6) Cooper, C. A.; Young, R. J.; Halsall, M. *Composites, Part A* **2001**, *32*, 401−411.
(7) Gierlinger, N.; Schwanninger, M.; Reinecke, A.; Burgert, I. *Biomacromolecules* **2006**, *7*, 2077−2081.
(8) Eichhorn, S. J.; Sirichaisit, J.; Young, R. J. *J. Mater. Sci.* **2001**, *36*, 3129−3135.
(9) Eichhorn, S. J.; Hughes, M.; Snell, R.; Mott, L. *J. Mater. Sci. Lett.* **2000**, *19*, 721−723.
(10) Peetla, P.; Schenzel, K. C.; Diepenbrock, W. *Appl. Spectrosc.* **2006**, *60*, 682−691.
(11) Quesada Cabrera, R.; Meersman, F.; McMillan, P. F.; Dmitriev, V. *Biomacromolecules* **2011**, *12*, 2178−2183.
(12) Rusli, R.; Shanmuganathan, K.; Rowan, S. J.; Weder, C.; Eichhorn, S. J. *Biomacromolecules* **2010**, *11*, 762−768.
(13) Rusli, R.; Shanmuganathan, K.; Rowan, S. J.; Weder, C.; Eichhorn, S. J. *Biomacromolecules* **2011**, *12*, 1363−1369.
(14) Pullawan, T.; Wilkinson, A. N.; Eichhorn, S. J. *Compos. Sci. Technol.* **2010**, *70*, 2325−2330.
(15) Eichhorn, S. J.; Young, R. J. *Compos. Sci. Technol.* **2004**, *64*, 767−772.
(16) Mitra, V. K.; William M. Risen, J.; Baughman, R. H. *J. Chem. Phys.* **1977**, *66*, 2731−2736.
(17) Batchelder, D. N.; Bloor, D. *J. Polym. Sci.: Polym. Phys. Ed.* **1979**, *17*, 569−581.
(18) Tashiro, K.; Kobayashi, M. *Polym. Bull.* **1985**, *14*, 213−218.
(19) Hinterstoisser, B.; Åkerholm, M.; Salmen, L. *Biomacromolecules* **2003**, *4*, 1232−1237.
(20) Wiley, J. H.; Atalla, R. H. *Carbohydr. Res.* **1987**, *160*, 113−129.
(21) Eichhorn, S. J.; Young, R. J.; Yeh, W. *Text. Res. J.* **2001**, *71*, 121−129.
(22) Eichhorn, S. J.; Baillie, C. A.; Zafeiropoulos, N.; Mwaikambo, L. Y.; Ansell, M. P.; Dufresne, A.; Entwistle, K. M.; Herrera-Franco, P.; Escamilla, G. C.; Groom, L.; Hughes, M.; Hill, C.; Rials, T. G.; Wild, P. M. *J. Mater. Sci.* **2001**, *36*, 2107−2131.
(23) Bakri, B.; Eichhorn, S. *Cellulose* **2010**, *17*, 1−11.
(24) Baley, C. *J. Mater. Sci.* **2004**, *39*, 331−334.
(25) Hughes, M. *Compos. Interfaces* **2000**, *7*, 13−29.
(26) Weibull, W. *J. Appl. Mech.−Trans. ASME* **1951**, *18*, 293−297.
(27) Isogai, A.; Saito, T.; Fukuzumi, H. T. *Nanoscale* **2011**, *3*, 71−85.
(28) Iwamoto, S.; Kai, W.; Isogai, A.; Iwata, T. *Biomacromolecules* **2009**, *10*, 2571−2576.
(29) Sturcova, A. *Biomacromolecules* **2005**, *6*, 1055−1061.
(30) Eichhorn, S. J.; Davies, G. R. *Cellulose* **2006**, *13*, 291−307.
(31) Tanaka, F.; Iwata, T. *Cellulose* **2006**, *13*, 509−517.
(32) Santiago Cintron, M.; Johnson, G.; French, A. *Cellulose* **2011**, *18*, 505−516.
(33) Saito, T.; Nishiyama, Y.; Putaux, J.; Vignon, M.; Isogai, A. *Biomacromolecules* **2006**, *7*, 1687−1691.
(34) Garlotta, D. *J. Polym. Environ.* **2001**, *9*, 63−84.
(35) Hill, C. A. S.; Khalil, H.P.S. A.; Hale, M. D. *Ind. Crops Prod.* **1998**, *8*, 53−63.
(36) Hill, C. A. S.; Jones, D.; Strickland, G.; Cetin, N. S. *Holzforschung* **1998**, *52*, 623−629.
(37) Murray, T. F.; Staud, C. J.; Gray, H. L. *Ind. Eng. Chem., Anal. Ed.* **1931**, *3*, 269−273.
(38) Tanghe, L. J.; Genung, L. B.; Mench, W. J. In *Determination of Acetyl Content and Degree of Substitution of Cellulose Acetate*; Whistler, R. L., Green, J. W., BeMiller, J. N. Wolfrom, M. L., Eds.; Methods in Carbohydrate Chemistry; Academic Press, London: 1963; Vol. *III* Cellulose, pp 201−203.
(39) Tingaut, P.; Zimmermann, T.; Lopez-Suevos, F. *Biomacromolecules* **2010**, *11*, 454−464.
(40) Fordyce, C. R.; Genung, L. B.; Pile, M. A. *Ind. Eng. Chem., Anal. Ed.* **1946**, *18*, 547−550.
(41) Marquardt, D. W. *J. Soc. Ind. Appl. Math.* **1963**, *11*, 431−441.
(42) Fukuzumi, H.; Saito, T.; Okita, Y.; Isogai, A. *Polym. Degrad. Stab.* **2010**, *95*, 1502−1508.
(43) Guo, Y.; Wu, P. *Carbohydr. Polym.* **2008**, *74*, 509−513.
(44) Kondo, T.; Sawatari, C. *Polymer* **1996**, *37*, 393−399.
(45) Colom, X.; Carrillo, F. *Eur. Polym. J.* **2002**, *38*, 2225−2230.
(46) Quero, F.; Nogi, M.; Yano, H.; Abdulsalami, K.; Holmes, S. M.; Sakakini, B. H.; Eichhorn, S. J. *ACS Appl. Mater. Interfaces* **2010**, *2*, 321−330.
(47) Young, R. J.; Eichhorn, S. J. *Polymer* **2007**, *48*, 2−18.
(48) Cox, H. L. *Br. J. Appl. Phys.* **1952**, *3*, 72.
(49) I'Anson, S. J.; Sampson, W. W. *Compos. Sci. Technol.* **2007**, *67*, 1650−1658.
(50) Henriksson, M.; Berglund, L. A.; Isaksson, P.; Lindström, T.; Nishino, T. *Biomacromolecules* **2008**, *9*, 1579−1585.